

## Article

# Monitoring the Ambient Seismic Field to Track Groundwater at a Mountain–Front Recharge Zone

Quinn Buzzard<sup>1</sup>, Jeff B. Langman<sup>2,\*</sup> , David Behrens<sup>2</sup> and James G. Moberly<sup>3</sup> <sup>1</sup> Water Resources Program, University of Idaho, Moscow, ID 83844, USA<sup>2</sup> Department of Earth and Spatial Sciences, University of Idaho, Moscow, ID 83844, USA<sup>3</sup> Department of Chemical and Biological Engineering, University of Idaho, Moscow, ID 83844, USA

\* Correspondence: jlangman@uidaho.edu

**Abstract:** The heterogeneity of the fractured-basalt and interbedded-sediment aquifer along the eastern margin of the Columbia Plateau Regional Aquifer System has presented challenges to resource managers in quantifying recharge and estimating sustainable withdrawals. Previous studies indicated recharge pathways in alluvial sediments atop a mountain–front interface upgradient of the basalt flows. In this sedimentary zone, six seismic stations were deployed for one year to detect velocity changes in low-frequency seismic waves that could be correlated to changes in groundwater recorded by a well transducer near the center of the seismic station network. Waveforms in the 1–5 Hz range were recorded at each station to determine changes in wave velocities between station pairs and correlate these velocity changes to changes in groundwater levels. The velocity–groundwater relation allowed for estimation of daily groundwater levels beneath the seismic station network. Existing hydrogeologic information was used to estimate hydraulic gradients and hydraulic conductivities, which allowed for the calculation of the daily volume of recharge passing beneath the seismic stations and into the confined aquifer system. The daily recharge volumes across the seismic station network were summed for comparison of the total annual recharge calculated from the change in seismic wave velocities (154,660 m<sup>3</sup>) to a flow model calculation of recharge based on areal precipitation and infiltration (26,250 m<sup>3</sup>). The 6× greater recharge estimated from the seismic wave velocity changes for this portion of the recharge zone is attributed to preferential pathways of high hydraulic conductivity and greater depth associated with paleochannels beneath the seismic station network.

**Keywords:** groundwater recharge; ambient seismic field; passive monitoring



**Citation:** Buzzard, Q.; Langman, J.B.; Behrens, D.; Moberly, J.G. Monitoring the Ambient Seismic Field to Track Groundwater at a Mountain–Front Recharge Zone. *Geosciences* **2023**, *13*, 9. <https://doi.org/10.3390/geosciences13010009>

Academic Editors: Nicolò Colombani and Jesus Martinez-Frias

Received: 27 August 2022

Revised: 20 December 2022

Accepted: 23 December 2022

Published: 28 December 2022



**Copyright:** © 2022 by the authors. Licensee MDPI, Basel, Switzerland. This article is an open access article distributed under the terms and conditions of the Creative Commons Attribution (CC BY) license (<https://creativecommons.org/licenses/by/4.0/>).

## 1. Introduction

Groundwater is an important resource for municipal, agricultural, and industrial uses across Idaho, the United States, and the globe [1–4]. Since 1935, water levels have declined in the multi-aquifer system in the South Fork Palouse River Basin (Figure 1) located in the Palouse geographic region and eastern margin of the Columbia Plateau Regional Aquifer System [5–7]. The South Fork Palouse River Basin aquifer system is contained in the fractured basalts of the Columbia River Basalt Group (CRBG) and interbedded sediments of the Latah Formation (Figure 2) that compose the eastern portion of the basin, designated as the Moscow–Pullman Basin (MPB) [8–10]. Groundwater in the local basin provides a primary source for drinking water and irrigation [11] and is the sole source of municipal water in the MPB [12]. Extrapolation of current trends in declining groundwater levels indicates the possibility of insufficient groundwater resources to meet future community needs [13]. Quantification of recharge to the MPB aquifer system is necessary to evaluate sustainable withdrawals or potential water storage/recovery systems. This study was conducted to evaluate groundwater changes and quantify the annual recharge along a portion of a theorized recharge zone by passively monitoring the ambient seismic field and correlating changes in seismic wave velocities to changes in groundwater levels.

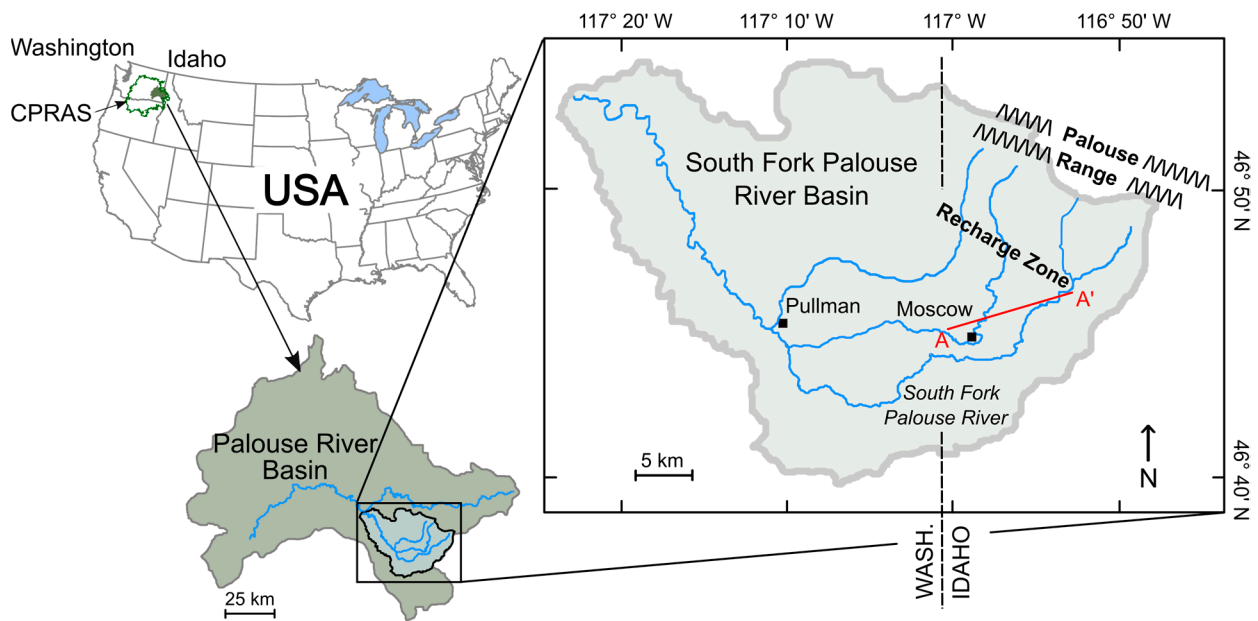


**Figure 1.** Location of the South Fork Palouse River Basin in the Palouse River Basin within the Columbia Plateau Regional Aquifer System (CPRAS) (modified from Behrens et al. [14]).

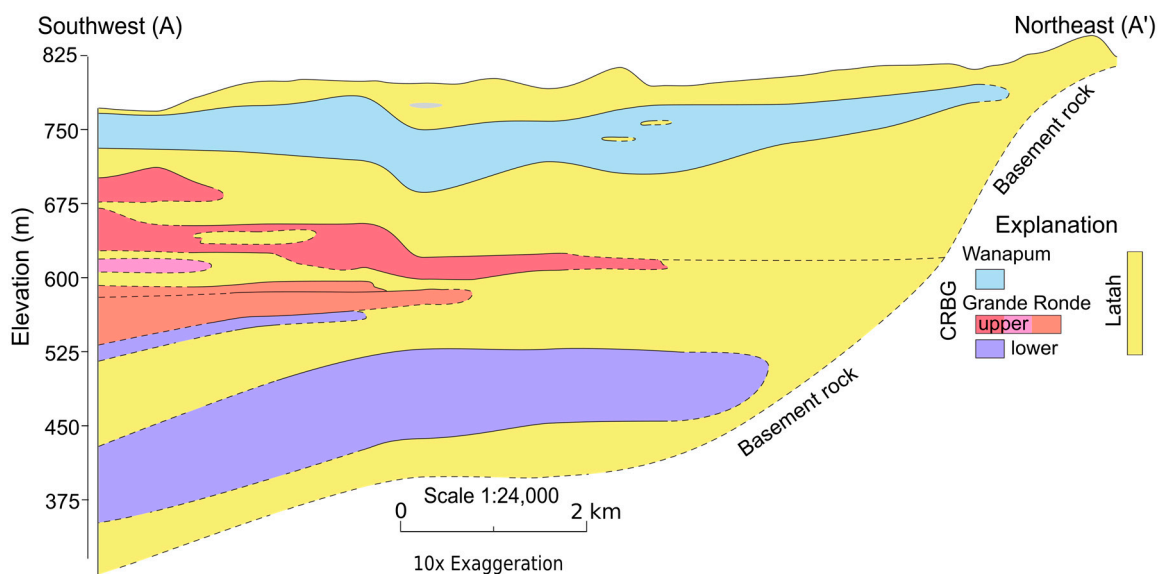


**Figure 2.** Southwest-to-northeast cross section (A–A', Figure 1) of the eastern South Fork Palouse River Basin near Moscow, Idaho, USA (modified from Bush et al. [9]).

Past modeling efforts to predict future declines in groundwater levels of the MPB have produced mixed results due to a limited understanding of recharge processes [15–19]. The variable permeability and discontinuity of basalt flows and interbedded sediments create heterogeneous and anisotropic aquifer matrices in the basin [10,20,21]. Resource management entities across the northwestern United States continue to struggle to model and predict recharge in such terrains [22]. An interstate, multi-agency committee of water providers in the MPB, Palouse Basin Aquifer Committee (PBAC), implemented a study to develop a new groundwater flow model to assist in understanding the continued decline in groundwater levels. As part of the modeling effort, recharge to the aquifer system was estimated by assigning a higher areal precipitation and infiltration rate to the foothill/mountainous region across the eastern portion of the basin (aligns with the recharge zone in Figure 1) and a lower rate for the lowlands of the basin [20]. This current

study was conducted to compare the annual recharge of the PBAC groundwater model in a portion of the recharge zone to the annual recharge calculated from groundwater levels derived from changes in the velocity of low frequency seismic waves recorded in the same portion of the recharge zone.

### 1.1. Recharge Zone

Previous studies have indicated that groundwater recharge (e.g., snowmelt) is entering the aquifer system through sediments of the Latah Formation [14,23–25] at the mountain–front interface along the eastern margin of the MPB [15,25–28]. These sediments overly the granitic basement rock at the mountain front of the Palouse Range (Figure 3). The sediments of the Latah Formation can range from permeable alluvial/colluvial deposits to clayey wetland deposits emplaced during damming of streams with the intrusion of CRBG flows [10]. Additionally, coarse paleochannel sediments are interspersed throughout the Latah Formation because of the continued rerouting of the paleostream network with the intrusion of at least 25 basalt flows [9,10]. The uppermost sediments of the Latah Formation can be clay rich but also contain coarser material that corresponds to the current stream network [9,10].

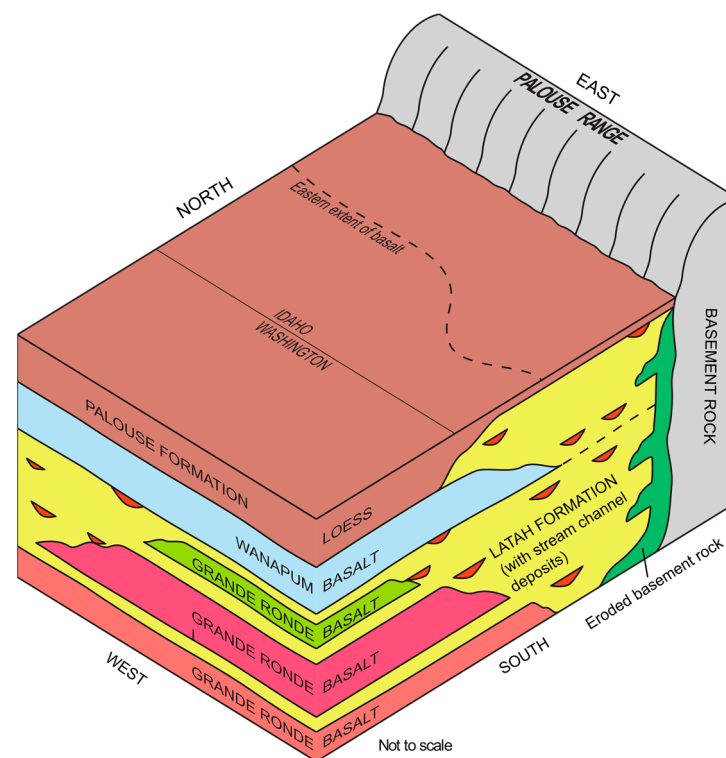


**Figure 3.** Theorized mountain–front interface of the Palouse Range and sedimentary units of the Latah Formation that contain paleochannel deposits from prior iterations of the stream network draining the Palouse Range (updated from Bush et al. [29]).

Downgradient of the theorized recharge zone, Duckett et al. [25] were able to discriminate two primary groundwater sources that originated from snowmelt moving either quickly into the subsurface (“fast pathway”) or snowmelt and/or rainfall that stayed in the surface-water network and entered the subsurface further downgradient (“slow pathway”). Behrens et al. [14] were able to refine the fast and slow pathway concept through an isotopic analysis of snowpack, snowmelt, runoff, creek, and groundwater samples collected from the mountain top to the recharge zone. The fastest recharge pathways appear to be located within the central portion of the recharge zone and slower pathways are located along the western and eastern peripheries [14]. These pathway types have some overlap with the

existing stream network but are not fully aligned, and the higher conductivity flowpaths in the recharge zone likely are associated with paleochannels [14].

### *1.2. Passive Seismic Monitoring for Estimating Groundwater Levels*

Passive seismic monitoring can be used to interpret near-surface conditions [30–34], such as changes in groundwater levels in unconfined and non-compartmentalized alluvial aquifers [35–37]. The scattering of seismic waves in the Earth’s crust allows for an averaged and volumetric view of changes in groundwater where the velocity of scattered seismic waves is sensitive to changes in pore pressure (e.g., grain-to-grain contact) [37–39]. Seismometers can be deployed to passively record low frequency waves of the ambient seismic field generated by natural or anthropogenic earth movements [40,41]. These low-frequency waves are influenced by the elastic properties of near surface materials and properties, such as changes in saturated thickness/pore pressure [37,38,40,42–46]. The velocity of scattered seismic waves in an aquifer will respond to changes in pore pressure caused by increased water levels and decreased grain contacts [36,38]. The recharge zone at the mountain front in the MPB is composed of unconsolidated sediments of the Latah Formation outside of the furthest extent of the basalts, which allowed for deployment of a temporary network of seismic stations to enhance the limited groundwater monitoring in this area (one well transducer).

## **2. Materials and Methods**

To quantify the annual recharge along a portion of the mountain–front recharge zone, six seismic stations were installed as a transect perpendicular to groundwater flow. This temporary seismic network was used to collect seismic spectra from October 2020 through September 2021 to correlate changes in seismic wave velocities to changes in groundwater levels. Available geologic data (e.g., well logs and local geologic reports) were used to interpret hydraulic gradients and hydraulic conductivities. The combination of groundwater levels/saturated thicknesses, hydraulic gradients, and hydraulic conductivities, allowed for estimating the volume of water passing beneath the seismic network and entering the MPB confined aquifer system during the study period.

### *2.1. Seismometer and Station Construction*

The Raspberry Shake<sup>®</sup> 1D was used for construction of the seismic stations. The Raspberry Shake<sup>®</sup> 1D contains a 4.5-Hz vertical geophone and internal memory for datalogging of up to 80 days. The geophone has the potential to resolve the low frequency range (0.1–5 Hz) that constitute the portion of the ambient seismic field that has previously been used to detect changes in seismic velocity because of changes in pore pressure/groundwater levels [31,37,45,47]. The seismometers were fitted with GPS units for an accurate record of time because of the need for cross-correlation analysis between stations for identifying changes in wave velocities [37,41,48,49]. The seismometer vaults (Figure 4) consisted of a weather-proof sealable container (action packer) for containing the seismometer in a weatherproof case and a deep cycle marine battery for power. The weatherproof case containing the seismometer was bolted to a granitic rock plinth and placed on a sand bed inside the action packer to ensure connection of the seismometer to the surrounding earth. The battery was connected to a solar panel (Figure 4) to reduce the need for battery replacement during the deployment period. Each seismic station was placed 1 m below land surface to connect with the surrounding earth and allow access to the seismometer. A data retrieval cable was paired with the power cable connecting the solar panel to the seismic station.



**Figure 4.** Seismic station composed of the buried, sealable container with solar panel and an inner view of the container with the marine battery and weatherproof case containing the seismometer.

## 2.2. Seismic Station Locations

Seismic station locations (Table 1) were based on proximity to the mountain front and outside the extent of the Wanapum basalt (Figure 3). Local drilling logs indicated that the selected sites likely had relatively shallow groundwater (<100 m) and relatively shallow basement rock (<500 m). One site was pre-selected because of an existing well containing an hourly recording Aqua4Plus 1.9.10 transducer (Figure 5) to which the seismic spectra were correlated for estimating groundwater across the seismic station network. The transducer well is 77 m deep and set in a mixed alluvium consisting of alternating clay- or gravel-rich layers that are part of the sediments of Bovill [9,24]. For quality control purposes, each seismic station was visited monthly for data downloading to ensure data preservation and identification of possible recording/power issues. If abnormal data output or power levels were detected, the vault was opened, and the instrumentation checked on-site.

**Table 1.** Seismic station location description.

Station ID	Latitude <sup>1</sup>	Longitude <sup>1</sup>	Elevation (m) <sup>2</sup>
1	46.78935	−117.010	848
2	46.78417	−116.987	853
3	46.77367	−116.975	824
4	46.77975	−116.972	848
5	46.77078	−116.951	846
6	46.76875	−116.936	863

<sup>1</sup> North American Datum of 1983 (NAD 83); <sup>2</sup> North American Vertical Datum of 1988 (NAVD 88).

## 2.3. Seismic Station Network and Quantifying Recharge

The seismic stations constituted a network of points overlying the non-compartmentalized sedimentary units composing the recharge zone, which connects the primary source water (e.g., infiltrated snowmelt at the mountain front) to the confined portion of the aquifer system. To correlate changes in seismic wave velocities and groundwater levels, the seismic station network was divided into station pairs and associated segments (Table 2 and Figure 5). Stations were paired by closest neighbor (west to east) for cross-correlation analysis of the waveforms recorded at each station. If a station could be paired to multiple stations (correlatable waveform distributions), each available pair was included in the analysis and recharge volumes from overlapping station pairs were averaged across the intersected area. From the station pairs and given sufficient ambient waveforms, a change

in velocity relative to velocity ( $dv/v$ ) can be used to determine groundwater levels [37]. Such a correlation is possible because the velocity of ambient waves is sensitive to changes in pore pressure with increasing or decreasing groundwater levels [38]. The velocity comparison ( $dv/v$ ) is a relativistic determination of waveform velocity differences recorded across the paired stations and represents a perturbation in the waveform velocity due to a change in groundwater levels that influence grain-to-grain contact from changes in pore pressure [37].

**Table 2.** Station pairs and associated network segments.

Station pairs	1–2	2–3	2–4	3–5	4–5	5–6
Recharge segments	A	B <sup>1</sup>	C <sup>1</sup>	D <sup>1</sup>	E <sup>1</sup>	F

<sup>1</sup> Overlapping station pairs were averaged for recharge calculations.

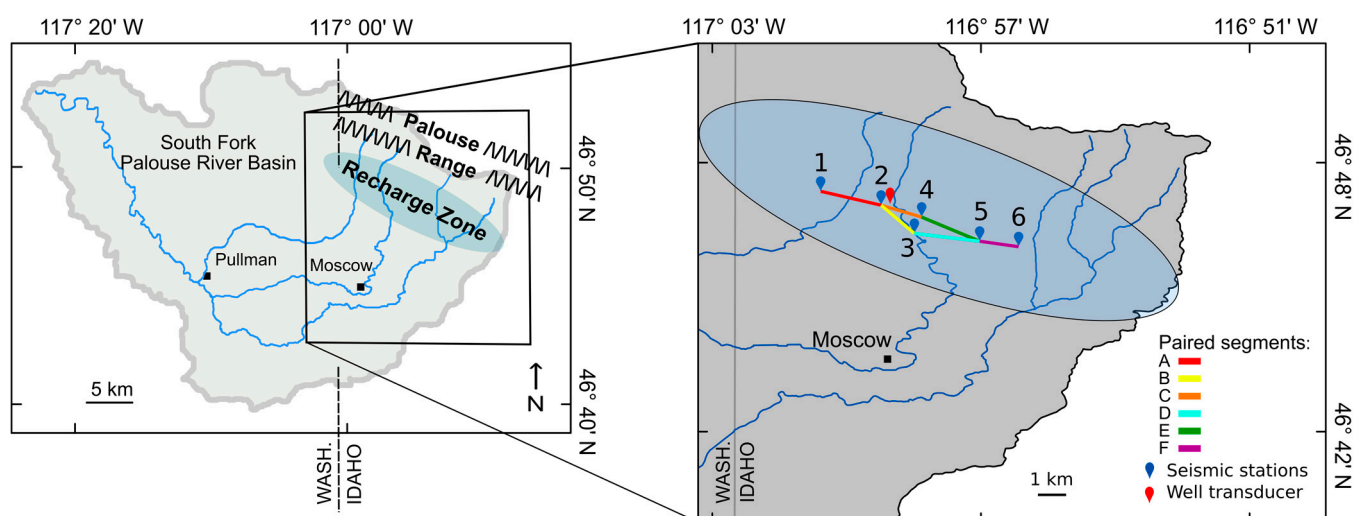


**Figure 5.** Seismic station locations and station pairs (paired segments) in the study area that is part of the theorized recharge zone along the Palouse Range.

#### 2.4. Identifying Applicable Waveforms in the Ambient Seismic Field

The waveforms from each seismic station were evaluated in ObsPy [50] with probabilistic power spectral density (PPSD) plots [51], which provided a view of smoothed and binned power spectral densities. These plots assisted in determining if low frequency waves were consistently detected by each seismometer. The 1–5 Hz range proved to be the most consistent waveform range at each station, which is within the applicable range for detecting changes in saturated thickness/pore pressure [37]. Small periods (hours to a few days) of data loss occurred at most seismic stations because of data corruption, but these short periods were linearly interpolated using the preceding and following changes in velocity. The percent of missing data ranged from 0% (segment F) to 11.8% (segment A) with an average data loss of 4.4%.

The cross-correlation function of MsNoise [52] was used to identify similar waveforms recorded between stations to create a proxy of Green's function. A whitening filter from 1–5 Hz was applied to correct for frequency attenuation of the recorded waves in this target range [53,54]. The cross-correlation functions between each station pair were computed at 1 h intervals with a 30 min overlap [37]. A 14-day stack of cross-correlation functions was used to maximize temporal resolution while minimizing spurious oscillations. A moving window cross spectral (MWCS) technique [37,55] was used to evaluate the delay in arrival times (change in time relative to time or  $dt/t$ ) for waveforms in the 1–5 Hz target range. It is assumed that there is a linear relation between relative time lags and seismic wave velocity changes (change in velocity relative to velocity or  $dv/v$ ), or  $-dt/t = dv/v$  [37,41,54,56].

### 2.5. Velocity Changes to Groundwater Levels

The groundwater level (GWL) between each station pair was derived through correlation of station pair  $dv/v$  and groundwater levels recorded by the well transducer near the center of the network. A single transducer recording groundwater levels can be reflective of changes in saturated thickness across a seismic station network overlying a non-compartmentalized alluvial aquifer (no barriers to recharge and GWL changes across the sedimentary units composing the aquifer) [37]. Estimates of GWL were calculated for each day at each station pair to produce daily groundwater values across the seismic station network for estimating the annual recharge volume. To correlate  $dv/v$  to groundwater, the relative changes had to be correlated within distinct seasonal periods. The  $dv/v$ -groundwater relations were assumed linear during the seasonal periods (rising or falling on a seasonal basis) and reflective of the elastic properties of the aquifer [37,40,57]. The study time frame was divided into four periods that correlate with periods of seasonal precipitation and infiltration or the lack of precipitation and infiltration: the end of the dry season and return of rainfall (October or period 1), winter snowfall/snowmelt (November through May or period 2), spring/summer snowmelt (June or period 3), and the dry summer season (July through September or period 4). These divisions align with basin precipitation patterns and subsequent streamflow and mountain-front groundwater response as monitored by the Natural Resources Conservation Service [58] and identified by past research in the basin [1,14,20,59]. The linear relation of groundwater changes ( $\Delta GWL$ ) and  $dv/v$  changes ( $\Delta dv/v$ ) were calculated from the period difference (maximum value – minimum value) of each seasonal period to determine the applicable correlation constant ( $C_{\text{period}}$ ):

$$\frac{GWL_{\text{max}} - GWL_{\text{min}}}{dv/v_{\text{max}} - dv/v_{\text{min}}} = \frac{\Delta GWL}{\Delta dv/v} = C_{\text{period}} \quad (1)$$

The daily  $dv/v$  change ( $\Delta dv/v_{\text{day}}$ ) was calculated by the difference between the initial  $dv/v$  of the period and a specific day  $dv/v$ :

$$dv/v_{\text{initial}} - dv/v_{\text{day}} = \Delta dv/v_{\text{day}} \quad (2)$$

The daily change in groundwater level ( $\Delta GWL_{\text{day}}$ ) was derived from the  $C_{\text{period}}$  and the  $\Delta dv/v_{\text{day}}$ :

$$\Delta dv/v_{\text{day}} \times C_{\text{period}} = \Delta GWL_{\text{day}} \quad (3)$$

The  $\Delta GWL_{\text{day}}$  was added to the initial period groundwater level ( $GWL_{\text{initial}}$ ) measured by the transducer to obtain the daily groundwater level ( $GWL_{\text{day}}$ ) for each station pair:

$$\Delta GWL_{\text{day}} + GWL_{\text{initial}} = GWL_{\text{day}} \quad (4)$$

### 2.6. Interpretations of Hydraulic Conductivity, Gradient, and Recharge

By discriminating sedimentary layer composition beneath seismic stations from local well logs and geologic reports [9,10,60,61], a composite hydraulic conductivity ( $K$ , m/d) was assigned for each station pair according to accepted  $K$  values for such alluvium types [62,63]. Given the unconfined alluvial aquifer of the recharge zone, hydraulic gradients ( $\Delta h/L$ ) were assumed to correspond to basement rock gradients beneath each station pair. The  $\Delta h/L$  of groundwater passing beneath each station pair were estimated from well logs above and below each station pair (depth to bedrock and linear interpretation of depth perpendicular to the station pair) and checked against the bedrock gradient derived by Bush et al. [10]. The  $\Delta h/L$  values ranged from 0.03 to 0.08 and correspond to the land surface gradient with the transition from the steeper mountain slope of the Palouse Range to the basin floor [10]. With calculation of daily groundwater levels from  $dv/v$  and depth to basement rock from the well logs, the daily saturated thickness could be calculated for each network segment (depth  $\times$  segment length = area ( $A$ ) in  $m^2$ ). Given  $K$ ,  $\Delta h/L$ , and  $A$ , the daily volume of recharge ( $Q$ ,  $m^3/d$ ) passing beneath each network segment was calculated using Darcy's law ( $Q = A \times K \times \Delta h/L$ ).

### 3. Results

#### 3.1. Velocity Changes and Relation to Groundwater

Changes in seismic velocity varied between station pairs (Figure 6) and ranged from a  $dv/v$  high of +0.45% (period 4) to a  $dv/v$  low of  $-0.3\%$  (period 2). The velocity changes inversely reflected the seasonal changes (rising or falling during the seasonal period) in groundwater elevation that ranged between 791 m and 795 m (Figure 6). The recorded changes in groundwater levels were representative of historical annual changes recorded at the transducer well location near the center of the transducer network. The  $dv/v$  values were lowest during periods of higher groundwater elevation (period 2 or the winter/spring snowmelt season) and highest during the dry periods (periods 1 and 4) that produced lower groundwater elevations (Figure 6). This inverse relation of  $dv/v$  and groundwater elevation corresponds to the expected changes in low-frequency wave velocities with changes in saturated thickness [37,40,45]. The seasonal flux of groundwater at the transducer represents the expected seasonal flux of recharge to the aquifer that is primarily driven by fall rainfall and winter/spring snowmelt [1,14,59].

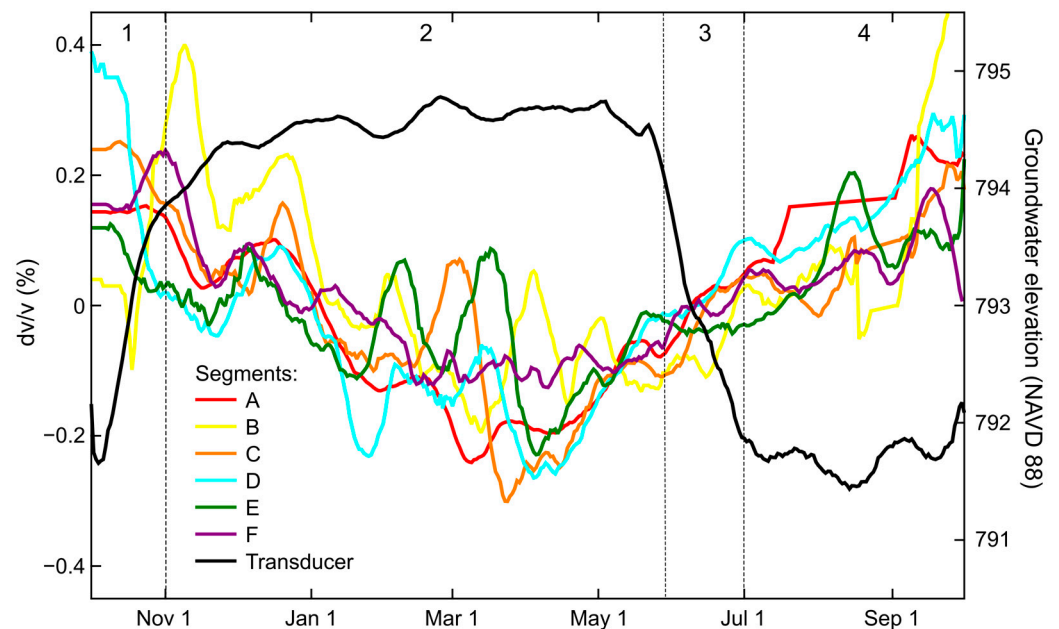


**Figure 6.** Changes in seismic velocity ( $dv/v$ ) at each network segment (Figure 5) and groundwater elevation recorded by the well transducer. Temporal periods (1–4) are seasonal divisions used to develop correlations between  $dv/v$  and groundwater changes for each seasonal period.

#### 3.2. Converting Seismic Velocity to Groundwater

The distinct seasonal periods in groundwater levels recorded by the transducer provided the necessary temporal periods for correlating  $dv/v$  and groundwater as separate seasonal relations (Table 3). The assumption of seasonal  $dv/v$ -groundwater relations parallels the seasonal flux of recharge that corresponds to surface hydrological processes of the basin [1,14,28,59]. The change in  $C_{\text{period}}$  (range of 4.6 to 37.3) reflects the high variability of groundwater levels/recharge during the 1-year study period (Table 3). Although the seasonal discrimination of the  $dv/v$ -groundwater relation provided a more refined correlation compared to an annual relation, groundwater elevations derived from  $dv/v$  tended to underestimate groundwater elevation during periods of increasing groundwater and overestimate groundwater elevation during periods of decreasing groundwater (Figure 7). These underestimation/overestimation periods represent a lag in the  $dv/v$ -groundwater relation following substantial changes in aquifer recharge (Figure 7). It is assumed that the lag period is an adjustment of overall grain-to-grain contact to the pore pressure changes reflective of the change in groundwater level.

**Table 3.** Seasonal periods and associated changes in groundwater ( $\Delta$ GWL) and seismic wave velocity ( $\Delta$ dv/v) for correlating ( $C_{\text{period}}$ ) the data sets and estimating groundwater levels.

Period	Date Range (2020–2021)	$\Delta$ GWL (m)	$\Delta$ dv/v (%)	$C_{\text{period}}$
1	October	+2.19	−0.07	31.2
2	November–May	+0.93	−0.20	4.6
3	June	−1.89	+0.05	37.3
4	July–September	−0.62	+0.12	5.3

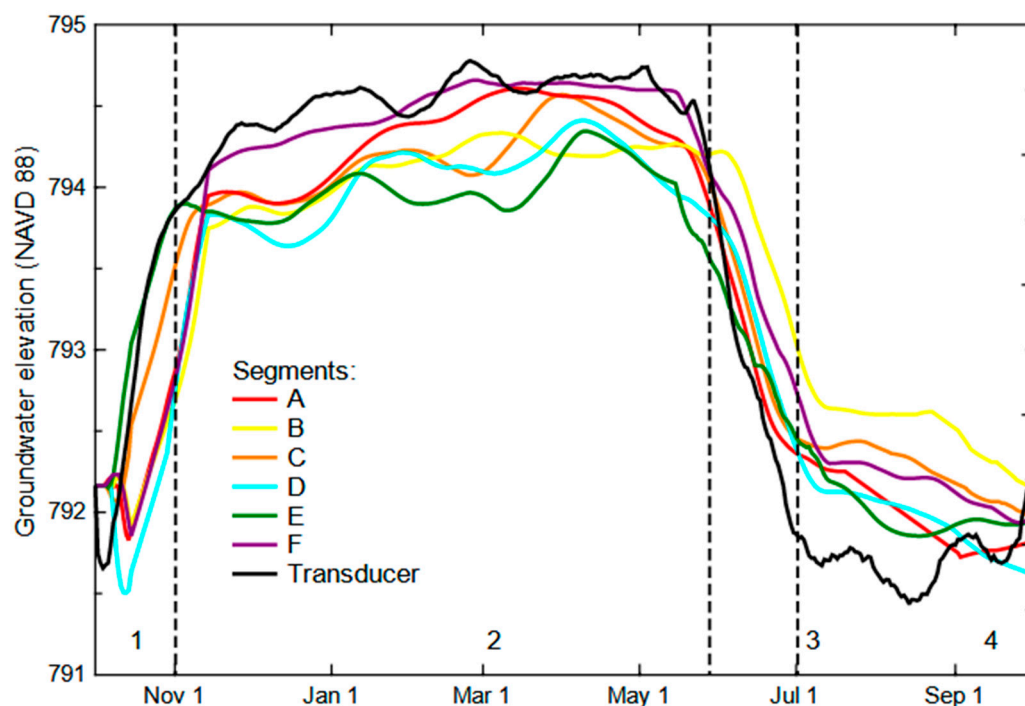


**Figure 7.** Groundwater elevations derived from dv/v for each network segment (Figure 5) compared to the groundwater elevation measured by the well transducer. Temporal periods (1–4) were seasonal divisions used to develop correlations between dv/v and groundwater changes.

### 3.3. Recharge Volumes by Network Segment

Interpretation of the well logs and geologic reports for evaluation of hydraulic conductivity (K) by network segment produced a range of segment composite K values from a low of 0.024 m/d (more clayey sediments of Bovill that are part of the Latah Formation [8]) to a high of 0.052 m/d (more paleochannel sand) (Table 4). These interpreted K values were calculated by the proportion of different sediment types estimated beneath each station or the mixture of lower conductivity alluvium (clayey) with paleochannel deposits (sand) and the presence of eroded basement rock (granular) [24]. The segment K values were smaller towards the west and largest on the east end of the seismic network. Hydraulic (bedrock) gradients also varied from low to high moving west to east with a corresponding increase in saturated thickness (Table 4). With the available groundwater levels (saturated thicknesses) across the seismic network and associated hydraulic conductivities and hydraulic gradients at each station pair, daily recharge volumes (example in Table 4) were calculated for each network segment and the overall seismic network (Figure 8). The average recharge volume was 422 m<sup>3</sup>/d with the largest recharge during period 2 (435 m<sup>3</sup>/d) and smallest during period 1 (404 m<sup>3</sup>/d) (Figure 8). Recharge was largest after a 10-day snowmelt period in early spring when approximately 15% of the mountain-snowpack water equivalent was lost [59]. Recharge volumes were smallest in period 1 following the summer dry season when <4 cm precipitation occurred in the preceding 3 months [59]. The total annual recharge for the recharge zone beneath the seismic network was estimated at 154,660 m<sup>3</sup>.

**Table 4.** Example of recharge calculations at each network segment and total recharge across the network for 1 October 2020. Overlapping segments were averaged for an adjusted recharge value.

Network Segment	Hydraulic Conductivity (m/d)	Saturated Thickness (m)	Station Distance (m)	Hydraulic Gradient	Potential Recharge (m <sup>3</sup> /d)	Adjusted Recharge <sup>1</sup> (m <sup>3</sup> /d)
A	0.024	8.0	1812	0.030	10.3	10.3
B <sup>1</sup>	0.033	17.8	1253	0.031	22.4	43.0
C <sup>1</sup>	0.033	23.5	1500	0.055	63.5	
D <sup>1</sup>	0.042	32.9	1883	0.080	210.6	189.8
E <sup>1</sup>	0.042	47.6	1927	0.044	169.0	
F	0.052	44.9	1130	0.063	164.6	164.6
Network sum (m <sup>3</sup> /d):						407.7

<sup>1</sup> Average recharge for overlapping network segments (Figure 5).

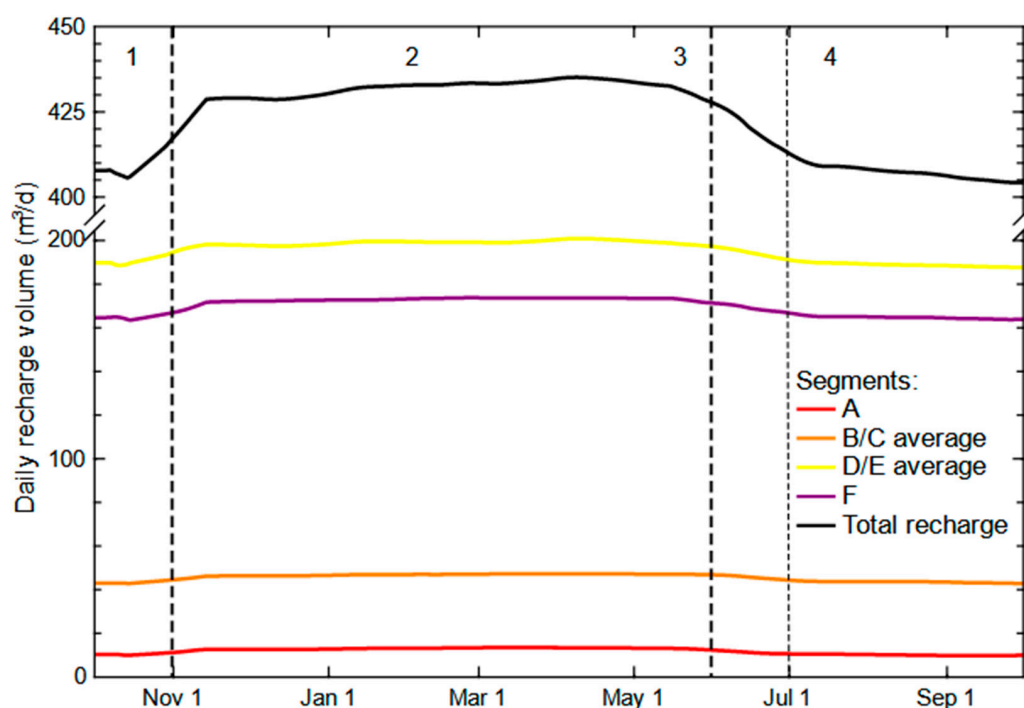


**Figure 8.** Daily recharge passing beneath the segments of the seismic network (Figure 5) and their summation from dv/v-derived groundwater elevations. Temporal periods (1–4) were seasonal divisions used to develop correlations between dv/v and groundwater changes.

**4. Discussion**

Recharge volumes were spatially variable across the seismic network with the largest volumes occurring in the central to eastern portion of the network because of greater saturated thicknesses (deeper bedrock), higher hydraulic conductivities (coarser grains from the presence of paleochannels), and steeper hydraulic gradients. This portion of the network (segments D/E and F) constituted 86% of the annual recharge volume while comprising about 50% of the network. The coarser grains, larger hydraulic conductivities, and steeper gradients of the eastern portion of the seismic network suggest faster recharge pathways, which aligns with the theorized fast recharge pathway identified for this area by Behrens et al. [14]. This faster pathway was assumed to be dominated by a greater concentration of paleochannels, which aligns with the review of sedimentary layer composition beneath this portion of the seismic network. The deeper bedrock of this area suggests greater erosion of the mountain front and correlates with the greater concentration of paleochannels and steeper gradients.

To compare the  $dv/v$ -derived recharge volume and the recharge volume derived by the PBAC groundwater model, the model aerial infiltration rate used for the foothills/mountainous region (105 mm/yr) was applied to the area from the seismic network to the upgradient watershed boundary for an annual estimate of 26,250 m<sup>3</sup>/yr. The larger estimate of recharge derived from the  $dv/v$  data (154,660 m<sup>3</sup>) is a reflection of greater saturated thicknesses and higher hydraulic conductivities paired with steeper hydraulic gradients, which align with the fast pathway concept of Duckett et al. [25] and Behrens et al. [14].

## 5. Conclusions

Discrimination of recharge pathways and quantification of recharge to the Moscow–Pullman Basin aquifer system in the Columbia Plateau Regional Aquifer System has posed challenges to resource managers due to the unique geology of the basin and limited well drilling in the theorized recharge zone. Such limitations have made it difficult to determine sustainable withdrawals from the aquifer system, which has undergone groundwater mining for a century. A recent groundwater modeling effort to assist with interpreting the effects of water conservation and withdrawal practices used an aerial infiltration method to estimate recharge along the eastern margin of the basin in a primary recharge zone. Six seismic stations were temporarily installed to enhance groundwater monitoring in a portion of the recharge zone and calculate an annual recharge to the confined aquifer system for comparison to recharge estimates from the groundwater model. Sufficient low-frequency seismic waves were recorded at the six seismic stations composing the seismic network for correlation to groundwater levels recorded by a well transducer located in the center of the network. Estimates of groundwater changes from changes in seismic wave velocities and estimates of hydraulic conductivities and hydraulic gradients from local well logs and geologic reports allowed for estimation of daily recharge volumes passing beneath the seismic network. Summation of the daily recharge estimates produced an annual recharge volume of 154,660 m<sup>3</sup>, which is six times greater than the model estimate of 26,250 m<sup>3</sup> for the same area. The larger estimate of recharge derived from the  $dv/v$  data is a reflection of a perceived faster pathway of recharge underlying a substantial portion of the seismic network. This faster pathway area highlights the variability of recharge pathways across the mountain front and the difficulty in modeling recharge in the basin.

**Author Contributions:** Conceptualization, J.B.L., D.B. and Q.B.; methodology, J.B.L. and Q.B.; software, J.G.M., Q.B., J.B.L. and D.B.; validation, Q.B., J.B.L. and J.G.M.; formal analysis, Q.B., J.B.L. and J.G.M.; investigation, Q.B. and J.B.L.; resources, Q.B., J.B.L. and J.G.M.; writing—original draft preparation, Q.B. and J.B.L.; writing—review and editing, Q.B., J.B.L. and J.G.M.; visualization, Q.B. and J.B.L.; supervision, J.B.L.; project administration, J.B.L.; funding acquisition, J.B.L. All authors have read and agreed to the published version of the manuscript.

**Funding:** This project was funded in part by the Palouse Basin Aquifer Committee.

**Data Availability Statement:** The data presented in this study are available upon request.

**Acknowledgments:** We acknowledge the support of the Palouse Basin Aquifer Committee to make this research possible. Special thanks to all the private landowners around Moscow who kindly allowed the installation of seismometers on their property.

**Conflicts of Interest:** The funding agency had no role in the design of the study; in the collection, analyses, or interpretation of data; in the writing of the manuscript, or in the decision to publish the results.

## References

1. Candel, J.; Brooks, E.; Sánchez-Murillo, R.; Grader, G.; Dijkma, R. Identifying Groundwater Recharge Connections in the Moscow (USA) Sub-Basin Using Isotopic Tracers and a Soil Moisture Routing Model. *Hydrogeol. J.* **2016**, *24*, 1739–1751. [[CrossRef](#)]
2. Custodio, E. *Trends in Groundwater Pollution: Loss of Groundwater Quality & Related Services*; Global Environment Facility and the Food and Agriculture Organization of the United Nations: Barcelona, Spain, 2014.
3. Llamas, M.; Custodio, E. *Intensive Use of Groundwater: Challenges and Opportunities*; A.A. Balkema Publishers: Madrid, Spain, 2002.

4. Gleeson, T.; Wada, Y.; Bierkens, M.F.P.; van Beek, L.P.H. Water Balance of Global Aquifers Revealed by Groundwater Footprint. *Nature* **2012**, *488*, 197–201. [[CrossRef](#)] [[PubMed](#)]
5. Foxworthy, B.L.; Washburn, R.L. *Ground Water in the Pullman Area, Whitman County, Washington*; U.S. Geological Survey: Washington, DC, USA, 1963.
6. Robischon, S. *Annual Water Use Report 2016*; Palouse Basin Aquifer Committee: Moscow, ID, USA, 2016.
7. Burns, E.R.; Snyder, D.T.; Haynes, J.V.; Waibel, M.S. *Groundwater Status and Trends for the Columbia Plateau Regional Aquifer System, Washington, Oregon, and Idaho*; U.S. Geological Survey: Washington, DC, USA, 2012.
8. Bush, J.H.; Pierce, J.L.; Potter, G.N. *Bedrock Geologic Map of the Moscow East Quadrangle, Latah County, Idaho*; Idaho Geological Survey: Moscow, ID, USA, 2010.
9. Bush, J.H.; Dunlap, P.; Reidel, S.P.; Kobayashi, D. *Geologic Cross Sections Across the Moscow-Pullman Basin, Idaho and Washington*; Idaho Geological Survey: Moscow, ID, USA, 2018.
10. Bush, J.H.; Dunlap, P.; Reidel, S.P. *Miocene Evolution of the Moscow-Pullman Basin, Idaho and Washington*; Idaho Geological Survey: Moscow, ID, USA, 2018.
11. Reidel, S.P.; Tolan, T.L.; Hooper, P.R.; Beeson, M.H.; Fecht, K.R.; Bentley, R.D.; Anderson, J.L. The Grande Ronde Basalt, Columbia River Basalt Group; Stratigraphic Descriptions and Correlations in Washington, Oregon, and Idaho. In *Volcanism and Tectonism in the Columbia River Flood-Basalt Province*; Geological Society of America: McLean, VA, USA, 1989; Volume 239, pp. 21–54.
12. Beall, A.; Fiedler, F.; Boll, J.; Cosens, B. Sustainable Water Resource Management and Participatory System Dynamics. Case Study: Developing the Palouse Basin Participatory Model. *Sustainability* **2011**, *3*, 720–742. [[CrossRef](#)]
13. Dhungel, R.; Fiedler, F. Water Balance to Recharge Calculation: Implications for Watershed Management Using Systems Dynamics Approach. *Hydrology* **2016**, *3*, 13. [[CrossRef](#)]
14. Behrens, D.; Langman, J.B.; Brooks, E.S.; Boll, J.; Waynant, K.; Moberly, J.G.; Dodd, J.K.; Dodd, J.W. Tracing  $\delta^{18}\text{O}$  and  $\delta^2\text{H}$  in Source Waters and Recharge Pathways of a Fractured-Basalt and Interbedded-Sediment Aquifer, Columbia River Flood Basalt Province. *Geosciences* **2021**, *11*, 400. [[CrossRef](#)]
15. Hernandez, H.P. Observations of Recharge to the Wanapum Aquifer System in the Moscow Area, Latah County, Idaho. Master's Thesis, University of Idaho, Moscow, ID, USA, 2007.
16. Kopp, W.P. Hydrogeology of the Upper Aquifer of the Pullman-Moscow Basin at the University of Idaho Aquaculture Site. Ph.D. Thesis, University of Idaho, Moscow, ID, USA, 1994.
17. Leek, F. Hydrogeological Characterization of the Palouse Basin Basalt Aquifer System, Washington and Idaho. Master's Thesis, Washington State University, Pullman, WA, USA, 2006.
18. Tong, L. Hydrogeologic Characterization of a Multiple Aquifer Fractured Basalt System. Ph.D. Thesis, University of Idaho, Moscow, ID, USA, 1991.
19. Lum II, W.E.; Smoot, J.L.; Ralston, D.R. *Geohydrology and Numerical Model Analysis of Ground-Water Flow in the Pullman-Moscow Area, Washington and Idaho*; US Geological Survey: Washington, DC, USA, 1990; p. 79.
20. Medici, G.; Engdahl, N.B.; Langman, J.B. A Basin-Scale Groundwater Flow Model of the Columbia Plateau Regional Aquifer System in the Palouse (USA): Insights for Aquifer Vulnerability Assessment. *Int. J. Environ. Res.* **2021**, *15*, 299–312. [[CrossRef](#)]
21. Medici, G.; Langman, J.B. Pathways and Estimate of Aquifer Recharge in a Flood Basalt Terrain; A Review from the South Fork Palouse River Basin (Columbia River Plateau, USA). *Sustainability* **2022**, *14*, 11349. [[CrossRef](#)]
22. Ryu, J.H.; Contor, B.; Johnson, G.; Allen, R.; Tracy, J. System Dynamics to Sustainable Water Resources Management in the Eastern Snake Plain Aquifer Under Water Supply Uncertainty1: System Dynamics to Sustainable Water Resources Management in the Eastern Snake Plain Aquifer Under Water Supply Uncertainty. *J. Am. Water Resour. Assoc.* **2012**, *48*, 1204–1220. [[CrossRef](#)]
23. Provant, A.P. Geology and Hydrogeology of the Viola and Moscow West Quadrangles, Latah County, Idaho and Whitman County, Washington. Master's Thesis, University of Idaho, Moscow, ID, USA, 1995.
24. Bush, J.H.; Dunlap, P. *Geologic Interpretations of Wells and Important Rock Outcrops in the Moscow-Pullman Basin and Vicinity, Idaho and Washington*; Idaho Geological Survey: Moscow, ID, USA, 2018.
25. Duckett, K.A.; Langman, J.B.; Bush, J.H.; Brooks, E.S.; Dunlap, P.; Welker, J.M. Isotopic Discrimination of Aquifer Recharge Sources, Subsystem Connectivity and Flow Patterns in the South Fork Palouse River Basin, Idaho and Washington, USA. *Hydrology* **2019**, *6*, 15. [[CrossRef](#)]
26. Ackerman, D.J. *Transmissivity of the Snake River Plain Aquifer at the Idaho National Engineering Laboratory, Idaho*; U.S. Geological Survey: Washington, DC, USA, 1991.
27. Duckett, K.A.; Langman, J.B.; Bush, J.H.; Brooks, E.S.; Dunlap, P.; Stanley, J.R. Noble Gases, Dead Carbon, and Reinterpretation of Groundwater Ages and Travel Time in Local Aquifers of the Columbia River Basalt Group. *J. Hydrol. Amst.* **2020**, *581*, 124400. [[CrossRef](#)]
28. Langman, J.B.; Martin, J.; Gaddy, E.; Boll, J.; Behrens, D. Snowpack Aging, Water Isotope Evolution, and Runoff Isotope Signals, Palouse Range, Idaho, USA. *Hydrology* **2022**, *9*, 94. [[CrossRef](#)]
29. Bush, J.H.; Dunlap, P.; Kodayashi, D. *A Collection of Geologic Maps, Cross Sections, and Schematic Diagrams That Illustrate the Subsurface Geology of the Moscow-Pullman Basin and Vicinity*; Palouse Basin Aquifer Committee: Moscow, ID, USA, 2019.
30. Bohnhoff, M.; Dresen, G.; Ellsworth, W.L.; Ito, H. Passive Seismic Monitoring of Natural and Induced Earthquakes: Case Studies, Future Directions and Socio-Economic Relevance. In *New Frontiers in Integrated Solid Earth Sciences*; Cloetingh, S., Negendank, J., Eds.; International Year of Planet Earth; Springer: Dordrecht, The Netherlands, 2010; pp. 261–285. ISBN 978-90-481-2737-5.

31. Mordret, A.; Courbis, R.; Brenguier, F.; Chmiel, M.; Garambois, S.; Mao, S.; Boué, P.; Campman, X.; Lecocq, T.; Van der Veen, W.; et al. Noise-Based Ballistic Wave Passive Seismic Monitoring—Part 2: Surface Waves. *Geophys. J. Int.* **2020**, *221*, 692–705. [[CrossRef](#)]
32. Meier, U.; Shapiro, N.M.; Brenguier, F. Detecting Seasonal Variations in Seismic Velocities within Los Angeles Basin from Correlations of Ambient Seismic Noise. *Geophys. J. Int.* **2010**, *181*, 985–996. [[CrossRef](#)]
33. Campillo, M.; Roux, P. Crust and Lithospheric Structure—Seismic Imaging and Monitoring with Ambient Noise Correlations. In *Treatise on Geophysics*; 2015; pp. 391–417, ISBN 978-0-444-53803-1.
34. McNamara, D.E.; Boaz, R.I. Visualization of the Seismic Ambient Noise Spectrum. In *Seismic Ambient Noise*; Nakata, N., Gualtieri, L., Fichtner, A., Eds.; Cambridge University Press: Cambridge, UK, 2019; ISBN 978-1-108-41708-2.
35. Grêt, A.; Snieder, R.; Scales, J. Time-Lapse Monitoring of Rock Properties with Coda Wave Interferometry. *J. Geophys. Res. Solid Earth* **2006**, *111*. [[CrossRef](#)]
36. Christensen, N.I.; Wang, H.F. The Influence of Pore Pressure and Confining Pressure on Dynamic Elastic Properties of Berea Sandstone. *Geophysics* **1985**, *50*, 207–213. [[CrossRef](#)]
37. Clements, T.; Denolle, M.A. Tracking Groundwater Levels Using the Ambient Seismic Field. *Geophys. Res. Lett.* **2018**, *45*, 6459–6465. [[CrossRef](#)]
38. Grêt, A.; Snieder, R.; Aster, R.C.; Kyle, P.R. Monitoring Rapid Temporal Change in a Volcano with Coda Wave Interferometry. *Geophys. Res. Lett.* **2005**, *32*. [[CrossRef](#)]
39. Christensen, N.I. The Influence of Pore Pressure on Oceanic Crustal Seismic Velocities. *J. Geodyn.* **1986**, *5*, 45–48. [[CrossRef](#)]
40. Lecocq, T.; Longuevergne, L.; Pedersen, H.A.; Brenguier, F.; Stammler, K. Monitoring Ground Water Storage at Mesoscale Using Seismic Noise: 30 Years of Continuous Observation and Thermo-Elastic and Hydrological Modeling. *Sci. Rep.* **2017**, *7*, 14241. [[CrossRef](#)]
41. Shapiro, N.M.; Campillo, M. Emergence of Broadband Rayleigh Waves from Correlations of the Ambient Seismic Noise. *Geophys. Res. Lett.* **2004**, *31*. [[CrossRef](#)]
42. Wang, Q.-Y.; Brenguier, F.; Campillo, M.; Lecointre, A.; Takeda, T.; Aoki, Y. Seasonal Crustal Seismic Velocity Changes Throughout Japan. *J. Geophys. Res. Solid Earth* **2017**, *122*, 7987–8002. [[CrossRef](#)]
43. Gassenmeier, M.; Sens-Schönfelder, C.; Delatre, M.; Korn, M. Monitoring of Environmental Influences on Seismic Velocity at the Geological Storage Site for CO<sub>2</sub> in Ketzin (Germany) with Ambient Seismic Noise. *Geophys. J. Int.* **2015**, *200*, 524–533. [[CrossRef](#)]
44. Tsai, V.C. Understanding the Amplitudes of Noise Correlation Measurements. *J. Geophys. Res. Solid Earth* **2011**, *116*. [[CrossRef](#)]
45. Voisin, C.; Guzmán, M.A.R.; Réfloch, A.; Taruselli, M.; Garambois, S. Groundwater Monitoring with Passive Seismic Interferometry. *J. Water Resour. Prot.* **2017**, *9*, 1414–1427. [[CrossRef](#)]
46. Garambois, S.; Voisin, C.; Romero Guzman, M.A.; Brito, D.; Guillier, B.; Réfloch, A. Analysis of Ballistic Waves in Seismic Noise Monitoring of Water Table Variations in a Water Field Site: Added Value from Numerical Modelling to Data Understanding. *Geophys. J. Int.* **2019**, *219*, 1636–1647. [[CrossRef](#)]
47. Prieto, G.A.; Denolle, M.; Lawrence, J.F.; Beroza, G.C. On Amplitude Information Carried by the Ambient Seismic Field. *Comptes Rendus Geosci.* **2011**, *343*, 600–614. [[CrossRef](#)]
48. Berryman, J.G. Seismic Wave Attenuation in Fluid-Saturated Porous Media. In *Scattering and Attenuations of Seismic Waves, Part I*; Aki, K., Wu, R.-S., Eds.; Pageoph Topical Volumes; Birkhäuser: Basel, Switzerland, 1988; pp. 423–432, ISBN 978-3-0348-7722-0.
49. Nakata, N.; Gualtieri, L.; Fichtner, A. *Seismic Ambient Noise*; Nakata, N., Gualtieri, L., Fichtner, A., Eds.; Cambridge University Press: Cambridge, UK, 2019; ISBN 978-1-108-41708-2.
50. Krischer, L.; Megies, T.; Barsch, R.; Beyreuther, M.; Lecocq, T.; Caudron, C.; Wassermann, J. ObsPy: A Bridge for Seismology into the Scientific Python Ecosystem. *Comput. Sci. Discov.* **2015**, *8*, 014003. [[CrossRef](#)]
51. McNamara, D.E.; Buland, R.P. Ambient Noise Levels in the Continental United States. *Bull. Seismol. Soc. Am.* **2004**, *94*, 1517–1527. [[CrossRef](#)]
52. Lecocq, T.; Caudron, C.; Brenguier, F. MSNoise, A Python Package for Monitoring Seismic Velocity Changes Using Ambient Seismic Noise. *Seismol. Res. Lett.* **2014**, *85*, 715–726. [[CrossRef](#)]
53. Sajid, M.; Ghosh, D. A Fast and Simple Method of Spectral Enhancement. *Geophysics* **2014**, *79*, V75–V80. [[CrossRef](#)]
54. Schimmel, M.; Stutzmann, E.; Ventosa, S. Low-Frequency Ambient Noise Autocorrelations: Waveforms and Normal Modes. *Seismol. Res. Lett.* **2018**, *89*, 1488–1496. [[CrossRef](#)]
55. Clarke, D.; Zaccarelli, L.; Shapiro, N.M.; Brenguier, F. Assessment of Resolution and Accuracy of the Moving Window Cross Spectral Technique for Monitoring Crustal Temporal Variations Using Ambient Seismic Noise. *Geophys. J. Int.* **2011**, *186*, 867–882. [[CrossRef](#)]
56. Sánchez-Sesma, F.J.; Campillo, M. Retrieval of the Green's Function from Cross Correlation: The Canonical Elastic Problem. *Bull. Seismol. Soc. Am.* **2006**, *96*, 1182–1191. [[CrossRef](#)]
57. Nanda, N.C. Seismic Wave and Rock-Fluid Properties. In *Seismic Data Interpretation and Evaluation for Hydrocarbon Exploration and Production: A Practitioner's Guide*; Nanda, N.C., Ed.; Advances in Oil and Gas Exploration & Production; Springer International Publishing: Cham, Switzerland, 2021; pp. 3–23, ISBN 978-3-030-75301-6.

58. National Water and Climate Center, NWCC Report Generator—Idaho SNOTEL Moscow Mountain Site, Average Precipitation Accumulation (1981–2010). Available online: [https://wcc.sc.egov.usda.gov/reportGenerator/view/customGroupByMonthReport/daily/989:id:SNL\T1\textbar{id=%22%22\T1\textbar{name/1980-10-01,1981-09-30/PREC::average\\_1981](https://wcc.sc.egov.usda.gov/reportGenerator/view/customGroupByMonthReport/daily/989:id:SNL\T1\textbar{id=%22%22\T1\textbar{name/1980-10-01,1981-09-30/PREC::average_1981) (accessed on 9 January 2019).
59. Sánchez-Murillo, R.; Brooks, E.S.; Elliot, W.J.; Boll, J. Isotope Hydrology and Baseflow Geochemistry in Natural and Human-Altered Watersheds in the Inland Pacific Northwest, USA. *Isotopes Environ. Health Stud.* **2015**, *51*, 231–254. [[CrossRef](#)]
60. Bush, J.H. *Bedrock Geologic Map of the Viola Quadrangle, Latah County, Idaho, and Whitman County, Washington*; Idaho Geological Survey: Moscow, ID, USA, 1998.
61. Pierce, J.L. *Geology and Hydrology of the Moscow East and Robinson Lake Quadrangles, Latah County, Idaho*. Master's Thesis, University of Idaho, Moscow, ID, USA, 1998.
62. Domenico, P.A.; Schwartz, F.W. *Physical and Chemical Hydrogeology*, 2nd ed.; Wiley & Sons: New York, NY, USA, 1997; ISBN 978-0-471-59762-9.
63. Freeze, R.A.; Cherry, J.A. *Groundwater*; Prentice-Hall: Englewood Cliffs, NJ, USA, 1979; ISBN 978-0-13-365312-0.

**Disclaimer/Publisher's Note:** The statements, opinions and data contained in all publications are solely those of the individual author(s) and contributor(s) and not of MDPI and/or the editor(s). MDPI and/or the editor(s) disclaim responsibility for any injury to people or property resulting from any ideas, methods, instructions or products referred to in the content.